Available online at www.sciencedirect.com
ScienceDirect
International Journal of Heat and Mass Transfer 51 (2008) 445–456
International Journal of HEAT and MASS TRANSFER
www.elsevier.com/locate/ijhmt

Atomistic simulation of rarefied gas natural convection in a finite enclosure using a novel wall-fluid molecular collision rule for adiabatic solid walls

P.Y. Tzeng [a], C.Y. Soong [b,*], M.H. Liu [c], T.H. Yen [d]

[a] Department of Aeronautical Engineering, Chung Cheng Institute of Technology, National Defense University, Tahsi, Taoyuan 33509, Taiwan, ROC
[b] Department of Aerospace and Systems Engineering, Feng Chia University Seatwen, Taichung 40724, Taiwan, ROC
[c] Planning Division, Army Headquarters, MND, Lungtan, Taoyuan 32509, Taiwan, ROC
[d] Graduate School of Defense Science Studies, Chung Cheng Institute of Technology, National Defense University, Tahsi, Taoyuan 33509, Taiwan, ROC

Received 19 November 2006; received in revised form 21 May 2007
Available online 30 July 2007

Abstract

In the present study, we propose a relatively novel wall-fluid molecule collision rule for description of adiabatic solid-wall in atomistic simulations and using it as boundary condition for simulation of rarefied gas natural convection in a finite enclosure of adiabatic sidewalls. This novel wall-fluid collision rule keeps the particle total velocity invariant and its normal velocity component reversed with the same magnitude before and after collision, while the other two components can vary randomly. This boundary treatment is more physically reasonable for description of a real solid-wall at adiabatic condition. To examine the performance of this novel rule, natural convection of rarefied gas in a micro-scale rectangular enclosure of length-to-height aspect ratios 2.016 and 4 heated from below is employed as the test model and predicted by direct simulation Monte Carlo (DSMC). The parameters of Knudsen number $Kn = 0.01$, 0.016, 0.02 and Rayleigh number Ra up to 3061 are considered. The present results demonstrate that the novel collision rule generates physically reasonable predictions of thermal-fluid behaviors at microscales and, compared to the existing boundary treatments of the same class, the present one is more efficient in the computational aspect.

Keywords: Wall-fluid molecular collision rule; DSMC; Rarefied gas; Microfluidics; Rayleigh–Bénard convection

1. Introduction

Due to rapid development of microsystem technology, in the recent two decades, study of flow characteristics at microscales has attracted lots of attentions [1]. In a micro flow configuration, the gaseous fluid flow cannot be regarded as continuum for its relatively large mean free path. Under this situation, atomistic methods have to be employed to perform simulation of the micro fluid behaviors. Molecular dynamics (MD) simulation [2–4] and direct simulation Monte Carlo (DSMC) [5,6] are two most commonly used methods in this aspect. In this class of simulation tools, MD is a deterministic method and mostly appropriate to the simulation of dense fluids or liquids such as water. The computational time needed in a MD simulation is proportional to the square of the number of the molecules in the fluid system. Therefore, the number of molecules has to be limited for its time-consumption. On the contrary, the strategy of the DSMC is to simulate tremendous amount of real molecules by small amount of particles, it means that the number of particles in DSMC can be relatively much less than that in MD simulation. Since DSMC employs method of probability to predict the occurrence of the molecule collisions with rarefied gas assumption of mean molecular spacing much larger than

* Corresponding author. Tel./fax: +886 4 24516246.
E-mail address: cysoong@fcu.edu.tw (C.Y. Soong).

0017-9310/$ - see front matter © 2007 Elsevier Ltd. All rights reserved.
doi:10.1016/j.ijheatmasstransfer.2007.05.011

Nomenclature

As	aspect ratio of enclosure, L/H
d	radius of molecule (m)
H	height of enclosure (m)
Kn	Knudsen number
L	width of enclosure (m)
m	mass of molecule (kg)
N_S	number of segments in Rapaport's model, $N_S = H/\delta$
n	number density (m^{-3})
p	pressure (Pa)
Ra	Rayleigh number
Ra_{C0}	Rayleigh number for onset of the convection at continuum condition
R_f	random number
r_{ref}	reference radius of molecules (m)
T	temperature (K)
V	pre-collision velocity vectors of fluid particle
V^*	post-collision velocity vectors of fluid particle
v_h	most probable thermal velocity at hot wall

Greek symbols

δ	segment length in Rapaport's model (m)
θ	dimensionless temperature, $\theta = (T - T_c)/(T_h - T_c)$
$\bar{\theta}$	horizontal average of dimensionless temperature
λ	mean free path of the molecule (m)
Ψ	dimensionless stream function
τ_t	mean collision time (s)
Δt	time step (s)

Subscripts

0	initial
c	cold
h	hot
R	right wall
M	middle point of the right-wall
m	maximum value

the effective molecular diameter. To deal with flow and heat transfer characteristics in a microscale gas flow configuration, DSMC is more appropriate than MD simulations [7,8].

In literature, the noted Rayleigh–Bénard (RB) convection in a rectangular enclosure is usually employed as a DSMC model for study of thermal-fluid characteristics in gaseous flow at microscales. The macro RB convection has been studied extensively in the past decades [8–13], whereas studies of the RB convection of rarefied gas appear only in the recent 15 years. Garcia [14] performed the first DSMC computation of the RB convection. Garcia and Penland [15] used principal oscillation pattern (POP) to analyze the data from DSMC and found that the DSMC results and the predictions of the linearized Navier–Stokes equations have very good qualitative agreement. Stefanov and Cercignani [16] explore effects of Knudsen number (Kn), Froude number and temperature difference between the top and bottom boundaries on the RB instability. Watanabe et al. [17] predict bifurcation of conductive to convective state of two-dimensional RB problem by DSMC with specular reflection at two sidewalls. The results revealed that, with diffuse condition posed on the top and bottom walls, the critical values of the governing parameter agree well with the counterpart case of the macro flow; while the critical parameter becomes higher as the semi-slip condition is used. The study of Yoshimura and Abe [18] disclosed that the rarefaction has stabilizing effect on Rayleigh–Bénard instability in an infinite fluid layer. Golshtein and Elperin [19] used DSMC combined with method of digital image filtering to eliminate statistical fluctuation as well as to reduce the computational time. The predictions of the critical parameter are lower than that from linear stability theory. Watanabe and Kaburaki [20] simulated three-dimensional RB system by parallel computation of DSMC. The critical values of the governing parameter found for appearance of hexagonal flow pattern are higher than predictions of linear stability theory.

Hirano et al. [21] demonstrated that the DSMC results approach the finite difference predictions of temperature and velocity fields as Kn decreases. Stefanov et al. [22,23] predicted periodic and chaotic attractors in mono-atomic rarefied gas RB instability problem by using DSMC. The predictions of critical condition at low Kn are very close to the threshold values found using finite difference method. Tzeng and Liu [24,25] explored effects of initial conditions, heating conditions, system dimensions, and number of particles on the RB flow patterns and found that the initial condition has noticeable influences on the flow pattern. Two side boundaries of the computational domain are subjected to specular reflection condition.

In the study of the macroscale two-dimensional RB instability/convection, it has been found that, stress-free condition on the top and bottom walls combined with two side boundaries periodic (symmetric), the critical Rayleigh number for onset of the convection is $Ra_{C0} = 657$. As the top and bottom walls are of no-slip in nature, the threshold becomes $Ra_{C0} = 1708$. The critical Rayleigh number becomes higher as the side boundaries are solid walls rather than the symmetric lines in fluids. Since the boundary conditions influence the RB instability/convection, simulation with correct boundary conditions is important.

In atomistic simulations, the diffuse reflection can be used to simulate rough surfaces, but there is energy

exchange between molecules and wall. It can be used for the solid wall with roughness but not appropriate for adiabatic walls. Specular reflection can be used for the boundaries at which the velocity and temperature fields both are symmetric, e.g., the boundaries of vortex-roll pairs in infinite RB problem. However, at adiabatic sidewalls of a solid enclosure, the temperature field has a zero gradient but the velocity is not. In this situation, both diffuse reflection and specular reflection are not appropriate. That means, in the aspect of atomistic simulation, the specular reflection is only good for a perfect smooth/slip surface but not a real solid-wall of roughness.

In all of the previous studies mentioned above, the specular reflection boundary condition was posed on the side boundaries. This specular reflection boundary condition is of course invalid for simulation of the RB convection in a finite solid box. Therefore, to find a solid-fluid collision rule considering a solid-wall at adiabatic condition is a significant issue of atomistic simulations. For MD study of RB convection in rectangular enclosures, Rapaport [26,27] adopted a segmented specular reflection boundary condition. The sidewalls were divided into a number of segments of length scale about one molecular radius. Each segment can be either specular reflection or velocity reversal. The two types of wall segments were arranged in a staggered mode. The previous results showed that this boundary condition is able to simulate no-slip adiabatic walls. However, in this boundary treatment, the reflection type of the colliding particle depends on the position where it collides with the wall.

Considering the conservation of energy with adiabatic condition and the randomness of the velocity components on a solid wall of roughness, we proposed a different wall-fluid collision model to simulate the adiabatic solid walls. The natural convection of rarefied gas in a micro-scale rectangular enclosure heated from below is simulated using DSMC with the present novel wall-fluid collision

Table 1
Boundary conditions used in DSMC for rarefied gas Rayleigh–Bénard convection

Authors (year)	*As*	*Kn*	Boundary conditions			
			Top	Bottom	Left	Right
Garcia (1990) [14]	1	0.029	Slip		Specular	
		0.02	Semi-Slip			
Garcia and Penland (1991) [15]	1	0.02	Slip		Specular	
Stefanov and Cercignani (1992) [16]	2, 3	0.01	Diffuse		Specular	
		0.02				
		0.05				
Watanabe et al. (1994) [17]	2.016	0.016	Diffuse		Specular	
	2.83		Semi-Slip	Diffuse	Specular	
Yoshimura and Abe (1995) [18]	2	0.025	Diffuse		Specular	
		~0.05				
Golshtein and Elperin (1996) [19]	5	0.01	Diffuse		Specular	
	2					
Watanabe and Kaburaki (1997) [20]	8:8:1	0.016	Diffuse		Specular	
	2:2:1					
Hirano et al. (2002) [21]	1	0.005	Diffuse		Specular	
		0.01				
		0.02				
		0.029				
Stefanov et al. (2002) [22,23]	2	0.001	Diffuse		Specular	
		~0.03				
Tzeng and Liu (2005) [24,25]	2, 4	0.01	Diffuse		Specular	
		~0.04				
Present Work	2.016, 4	0.01	Diffuse		Specular (SR)	
		0.016			Sg-SV [26,27]	
		0.02			Pt-SD (Novel)	

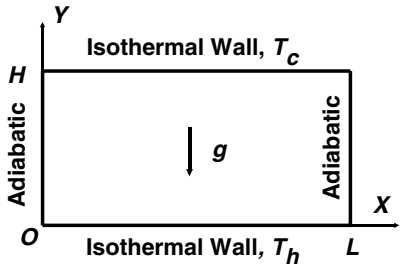

Fig. 1. Physical model of a two-dimensional rectangular enclosure of length L and height H with side walls adiabatic; the upper and bottom walls are isothermal at T_c and T_h, respectively.

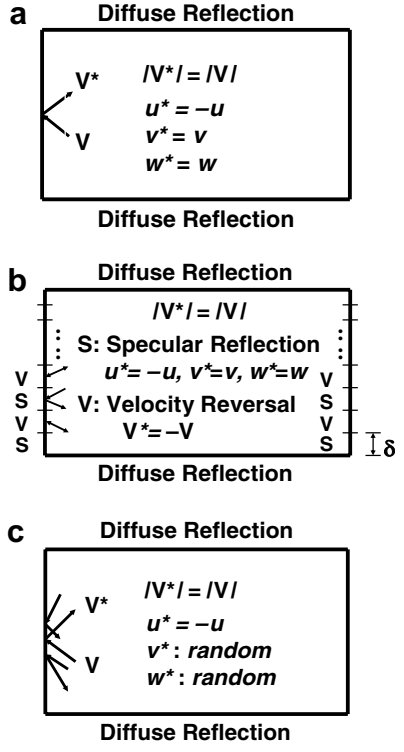

Fig. 2. Schematic diagram of the hybrid model of adiabatic boundary condition (a) SR BC, (b) Sg-SV BC, and (c) Pt-SD BC.

rule. Results generated with different boundary conditions are also compared. Table 1 presents boundary conditions used in previous studies of atomistic simulation for rarefied gas Rayleigh–Bénard convection.

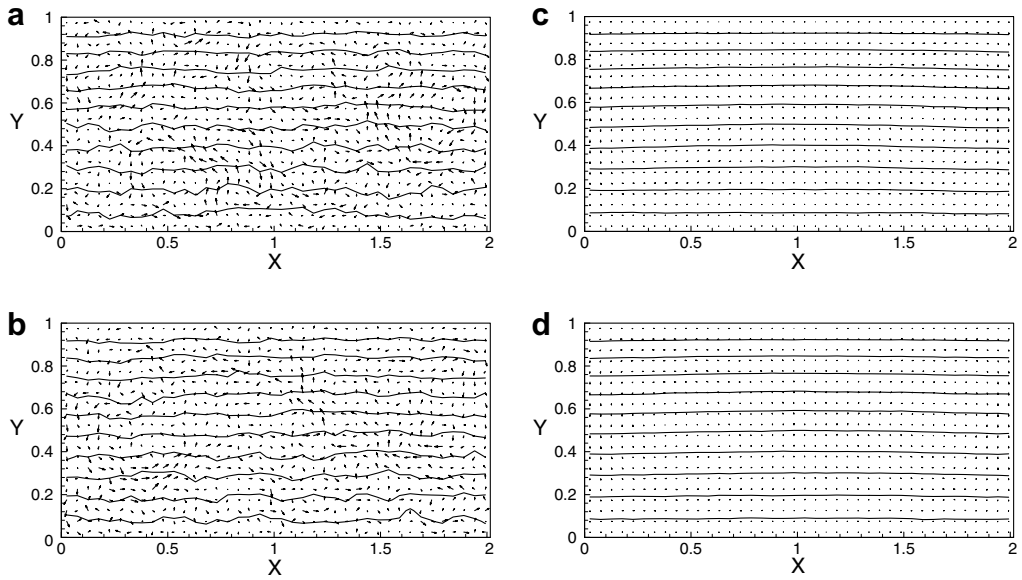

Fig. 3. Flow velocity vector fields and isotherms at $Kn = 0.016$ and (a) $Ra = 1507$ (Sg-SV BC), (b) $Ra = 1507$ (Pt-SD BC), (c) $Ra = 1646$ (Sg-SV BC), (d) $Ra = 1646$ (Pt-SD BC).

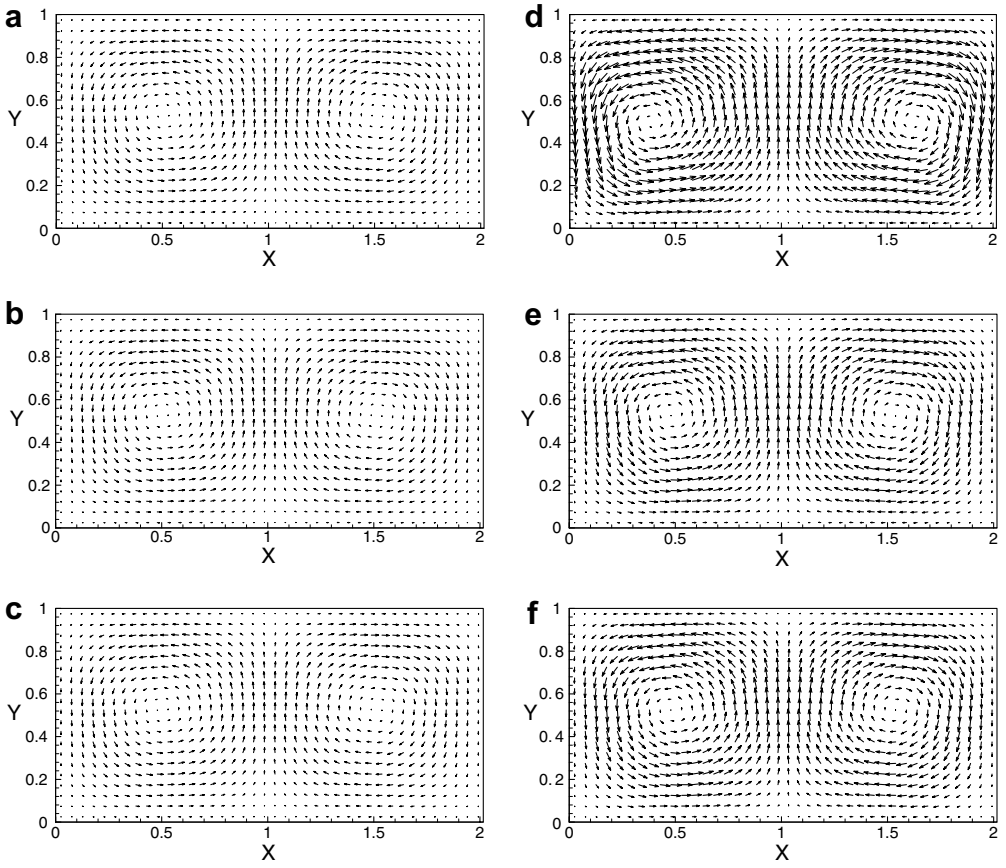

Fig. 4. Flow velocity vector fields in enclosure of $As = 2.016$ at $Kn = 0.016$ and (a) $Ra = 2632$ (SR BC), (b) $Ra = 2632$ (Sg-SV BC), (c) $Ra = 2632$ (Pt-SD BC), (d) $Ra = 3061$ (SR BC), (e) $Ra = 3061$ (Sg-SV BC), (f) $Ra = 3061$ (Pt-SD BC).

2. Physical model and boundary conditions

2.1. Thermal-fluid model – enclosure heated from below

The geometry and coordinate system of the 2D horizontal rectangular enclosure simulated in the present work are shown in Fig. 1. The flow configurations used by Watanabe et al. [17] are adopted. The computational domain is of height $H = 5.6 \times 10^{-3}$ m and width $L = 1.13 \times 10^{-2}$ m. The corresponding length-to-width aspect ratio is $As = L/H \simeq 2.016$, which is approximately the dimensionless wavelength at the theoretical critical Rayleigh number $= Ra_{C0} = 1708$. The gas under consideration is air of hard sphere (HS) model with mass $m = 4.8 \times 10^{-26}$ kg and molecular radius $d = 3.7 \times 10^{-10}$ m. The initial pressure and temperature are $p_0 = 20$ Pa and $T_0 = 80$ K, respectively. Under these conditions, the number density is $n_0 = 1.81 \times 10^{22}$ m^{-3}, the mean free path $\lambda_0 = 9.08 \times 10^{-5}$ m, and then the Knudsen number is $Kn = 0.016$. The top (cold) wall temperature lies at a constant and uniform temperature $T_c = 80$ K, while the bottom (hot) wall also at a constant and uniform temperature in the range of 100–600 K. The Rayleigh number Ra ranges from 126 to values over 3000.

The domain is divided into 40×20 sampling cells, and each sampling cell is further divided into 5×5 collision cells. Initially, 400 and 16 particles are uniformly distributed in the sampling and collision cell, respectively. The total number of the particle in the simulation is 3.2×10^5. As to the time step in the simulation, we adopt $\Delta t = 0.9\tau_t$, and $\tau_t = \lambda_0/v_h$ is the mean collision time and $v_h = (2k_B T_h/m)^{-1/2}$ is the most probable thermal velocity evaluated based on the hot wall temperature. In the computational process, sampling is performed every two time steps, and averaging is taken for every 100 sampling data. After 30,000 time steps, statistical mean of the fluid properties is performed till 50,000 time steps.

2.2. Boundary conditions

The pre- and post-collision velocity vectors of a fluid particle are denoted by $\mathbf{V} = u\mathbf{i} + v\mathbf{j} + w\mathbf{k}$ and $\mathbf{V}^* = u^*\mathbf{i} +$

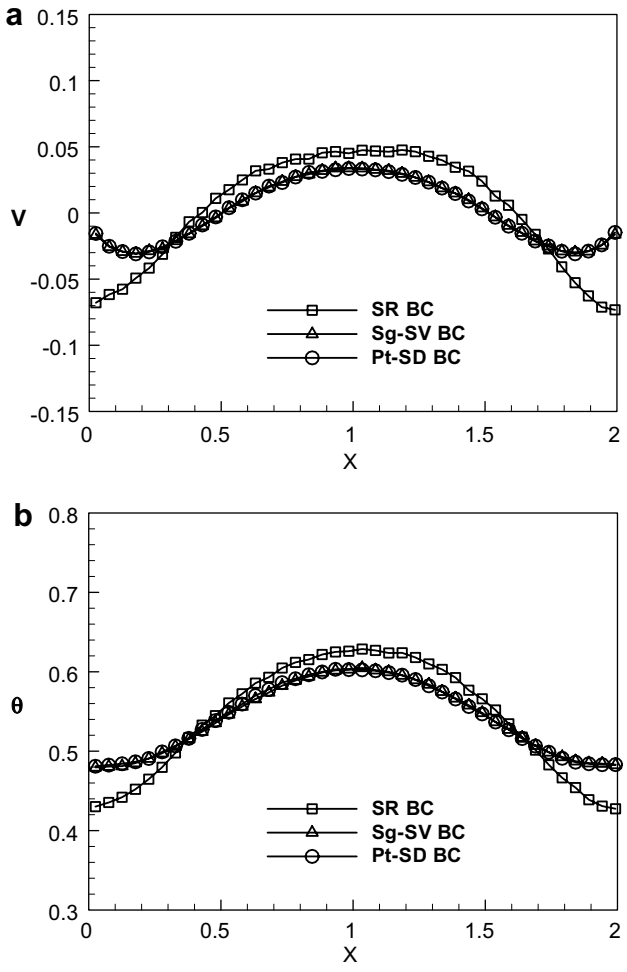

Fig. 5. Transverse velocity and temperature distributions at mid-level of the enclosure of $As = 2.016$ at $Kn = 0.016$ and $Ra = 2632$. (a) Transverse velocity and (b) temperature.

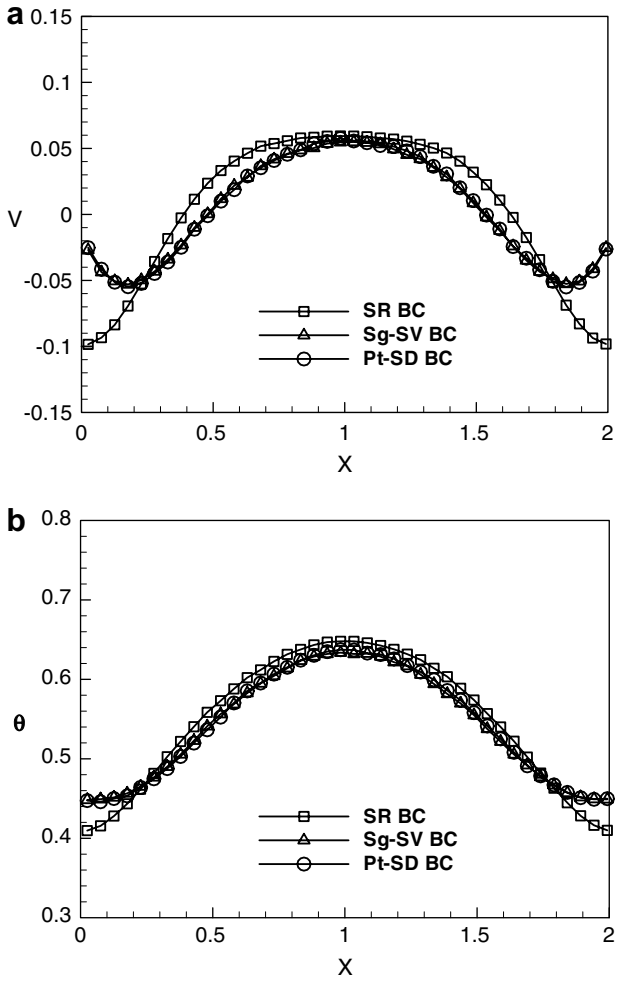

Fig. 6. Transverse velocity and temperature distributions at mid-level of the enclosure of $As = 2.016$ at $Kn = 0.016$ and $Ra = 3061$. (a) Transverse velocity and (b) temperature.

$v^*\mathbf{j} + w^*\mathbf{k}$, respectively. In general, the diffuse reflection is appropriate for an isothermal solid wall, whereas the specular reflection is inherently symmetric in nature. To meet the requirement of adiabatic condition, the energy has to be conserved, i.e., $|\mathbf{V}^*|^2 = |\mathbf{V}|^2$ or $|\mathbf{V}^*| = |\mathbf{V}|$. The major difference among various adiabatic wall conditions is the treatment of the velocity components. As mentioned earlier, this specular reflection boundary condition (SR BC) is basically valid for the boundaries where both velocity and temperature fields are symmetric but incorrect for thermally adiabatic condition at the solid wall. For the specular reflection as shown in Fig. 2a, the velocity components are all keep invariant in their magnitudes but normal component reversed in direction, i.e., $u^* = -u$, $v^* = v$, $w^* = w$.

To overcome this difficult situation in atomistic simulation, in their molecular dynamics simulation, Rapaport [25,26] proposed a segmented specular reflection/velocity reversal boundary condition (herein denoted as Sg-SV BC). As shown in Fig. 2b, the wall is divided into numerous segments, each segment is of length δ, which equals to the reference radius of molecules, r_{ref}. The number of the segment is $N_S = H/\delta$, and it is of order about 10^7. At each wall, from bottom to top, each segment is assigned specular reflection and velocity reversal in a staggered manner. Therefore, this boundary condition is herein denoted as Sg-SV BC. For the specular reflection segments, the velocity components can be depicted as that stated in last paragraph, whereas for velocity reversal segments, all velocity components of the particle before and after colliding with the wall are of the same magnitude but opposite direction, i.e., $\mathbf{V} = -\mathbf{V}^*$. At both the specular reflection and this velocity reversal conditions, the magnitude of the total velocity remains unchanged after colliding with the wall. Since there is no energy exchange between the particle and the wall, the solid wall is regarded as adiabatic. In addition, with segments of molecular size $\delta = r_{\text{ref}}$ and staggered arrangement of specular reflection and velocity reversal, the wall seems equivalent to a corrugated surface of roughness.

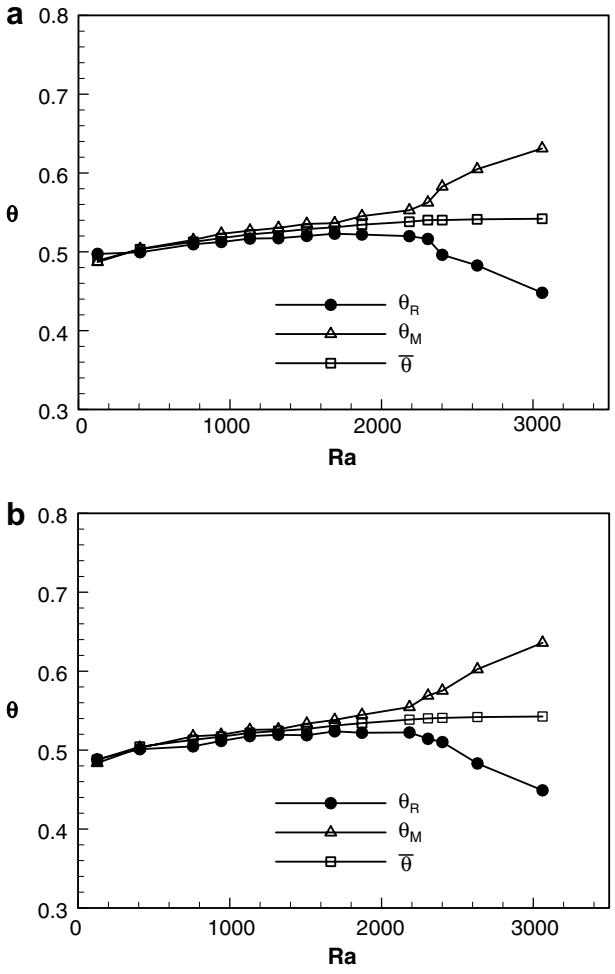

Fig. 7. Bifurcation diagrams for the flows at $Kn = 0.016$ in enclosure of $As = 2.016$ with sidewalls at (a) Sg-SV BC, (b) Pt-SD BC. (θ_R: right-side boundary, θ_M: in the middle of enclosure, $\bar{\theta}$: horizontal averaged).

In the present work, we propose a relatively novel boundary treatment, in which the reflected particle after colliding with the wall is also assumed to have the total energy unchanged, $|\mathbf{V}^*| = |\mathbf{V}|$. Different from the Rapaport's method, the collision rule is applied everywhere on the wall with the normal velocity reversal, $u^* = -u$, but the two velocity components tangential to the wall, v and w, reflecting randomly, *viz.*,

$$v^* = \sin(2\pi R_f)(|\mathbf{V}|^2 - u^2)^{1/2} \tag{1}$$

$$w^* = \cos(2\pi R_f)(|\mathbf{V}|^2 - u^2)^{1/2} \tag{2}$$

where R_f is a random number. Fig. 2c schematically presents this novel boundary treatment. In this novel collision rule, combination of the normal component reversal with random reflection of the molecule velocity components in the two directions tangential to the wall partially is employed to simulates the molecule reflection on a real surface. This treatment is a hybrid one with effects of partial specular and partial diffuse reflections and thus is denoted as Pt-SD BC hereafter.

The use of the normal velocity reversal, $u^* = -u$, seems not necessarily true for the particle collision on a rough wall. However, it is used as a mechanism to simulate the adiabatic solid wall, which is actually partial specular and partial diffuse in nature. Rapaport's proposal of a segmented specular reflection/velocity reversal condition also used $u^* = -u$. In addition, Yamamoto, et al. [28] in their recent work used the molecular dynamics (MD) simulation to study collisions of gas molecules with either clean or contaminated surface. Their results indicated that the global velocity distribution functions of the reflected molecules for gas-wall interactions are nearly symmetric to the distributions of the incident molecules and well described by the Maxwell-type reflection conditions. It implies that the average magnitude of the normal velocity component is most likely unchanged or changes little. For the present case of adiabatic wall, it seems reasonable to use this notion of approximately equal average normal velocity

components of incident and reflected molecules and to assume $u^* = -u$ for gas-wall collisions. Accordingly, the present collision rule invokes this normal velocity reversal condition with consideration of energy conservation and randomly changed tangential velocity components. Our proposal is able to satisfy the adiabatic condition and has some merits as compared with the previous method.

3. Results and discussion

In the enclosure of $As = 2.016$, velocity and temperature solutions at $Kn = 0.016$ and $Ra = 1507$ predicted using DSMC with Sg-SV BC and Pt-SD BC as the sidewall condition are presented in Fig. 3a and b. It is found that the two solutions are both at conduction state. As Ra increase up to 1646, the extremely weak convection roll emerge but the isotherms pattern still remains stratified just as that at a conduction state, see Fig. 3c and d. With increases in Ra up to $Ra = 2632$, the flow field solutions at three sidewall conditions, SR, Sg-SV, and Pt-SD, are presented in Fig. 4a–c. At this higher Ra, onset of the convection is obviously occurs and vortex rolls form. Further increases Rayleigh number to $Ra = 3061$, the flow fields with sidewall conditions of SR, Sg-SV, and Pt-SD in Fig. 4d–f demonstrate the increasingly strong convection in the enclosure. It is also observed that the solutions with SR BC are of stronger convection rolls and the solutions with boundary conditions of Sg-SV and Pt-SD are both of relatively weaker convection. The reason for this consequence is that the SR BC stands for symmetric but not solid boundaries; while the last two conditions model adiabatic solid walls. Physically, the confinement of the solid walls has a retarding effect on formation of the vortex rolls.

The velocity vector fields shown in Fig. 4 reveal only qualitative nature of the natural convection. To compare the differences among the solutions with three adiabatic sidewall conditions of SR, Sg-SV, and Pt-SD, a quantitative presentation of the field solutions is most useful. Figs. 5 and 6 present temperature and transverse velocity distributions at $Ra = 2632$ and 3061, respectively. In Fig. 5a, the transverse velocity distribution with SR BC shows larger fluid slippage as well as higher gradient in velocity distribution than the other two solutions. It implies that the SR BC solution represents a flow field of stronger convection. The larger difference between the local temperatures in central and near-wall regions is also an evidence for the existence of the strong convection effect, which can be found in the

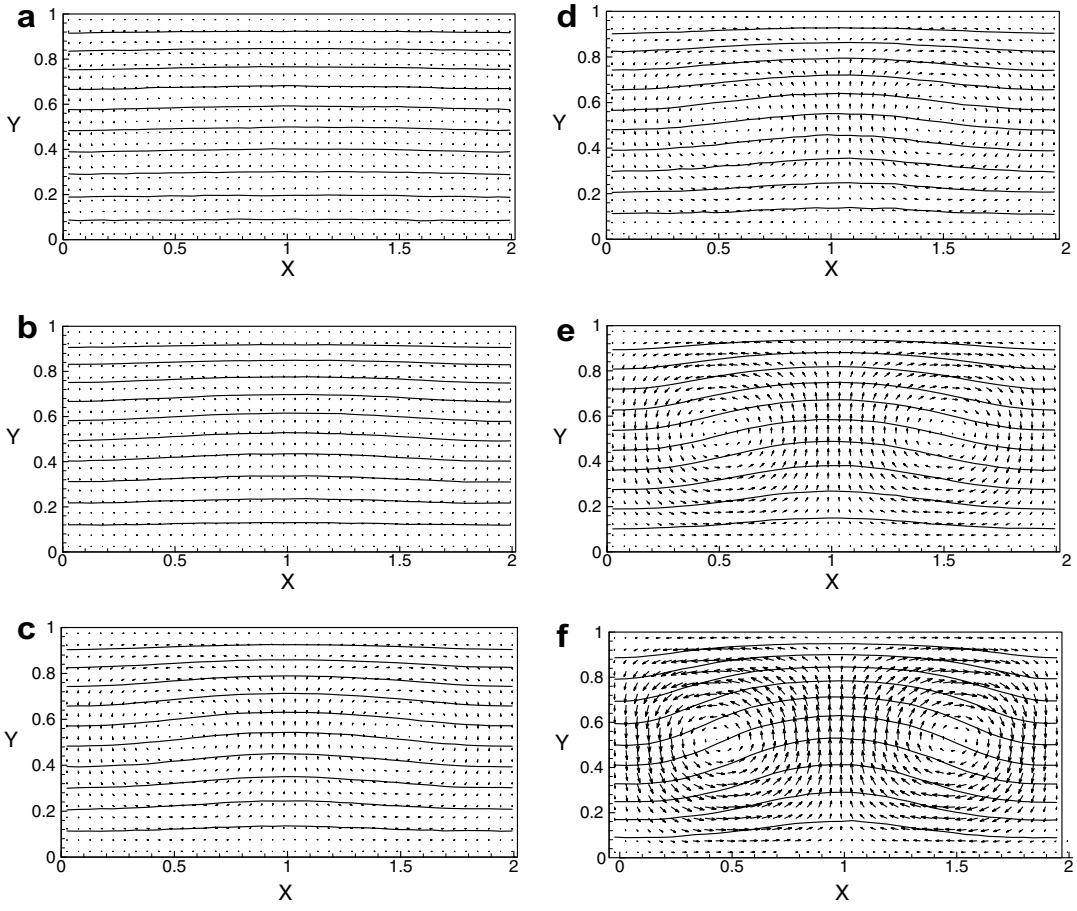

Fig. 8. DSMC predictions with Pt-SD BC at $Kn = 0.016$ in an enclosure of $As = 2.016$ at various Ra. (a) $Ra = 1646$, (b)$Ra = 2127$, (c) $Ra = 2300$, (d) $Ra = 2400$, (e) $Ra = 2632$, (f) $Ra = 3061$.

distorted temperature distribution shown in Fig. 5b. In addition, both the temperature profiles for SR BC and Pt-SD BC normal to the sidewalls, which is an evidence of adiabatic wall condition. Besides, the SR BC solution has more noticeable slippage on sidewalls. On the contrary, the Sg-SV BC and the Pt-SD BC proposed in the present work generate near-zero velocity (slip velocity) on sidewalls. It is believed that the conditions of Sg-SV and the Pt-SD are better for prescribing a solid wall. In the case of $Ra = 3061$ shown in Fig. 6, the similar effects can be found and even more obvious for this higher Ra.

Bifurcation diagrams for $Kn = 0.016$ with the temperatures on the middle point of the right-wall, θ_R, on the middle point of the enclosure, θ_M, and the horizontal average, $\bar{\theta}$, versus the governing parameter Ra are plotted in Fig. 7. Theoretically, the fluid layer between two parallel plates heat from below has critical condition $Ra = 2010$ and the corresponding wavelength is 2.016. From continuum computation for the solid enclosure of aspect ratio 2, the critical condition is $Ra = 2160$. The present predictions for the case of $Kn = 0.016$ with either Sg-SV or Pt-SD condition in Fig. 7 show that the threshold occurs in the range of Ra between 2000 and 2200. To provide a clearer picture about the variation of the thermal-fluid behaviors with Ra around threshold condition, the velocity vector fields and isotherms at $Ra = 1646$–3061 solved with the Pt-SD BC are presented in Fig. 8. By carefully inspecting the results shown in Fig. 8, it can be inferred that the onset of the convection in this case occurs at $Ra \approx 2120$.

In this rarefied gas flow configuration, particle motion is three-dimensional but, with periodicity in z-direction (perpendicular to the paper) as that treated in previous studies, the resultant bulk flow motion is presented as two-dimensional in x–y plane. Considering the density variation in the flow field, the stream function ψ is defined based on the velocity-stream function relationships for compressible flows, i.e., $\rho u = \partial\psi/\partial Y$ and $\rho v = -\partial\psi/\partial X$. Therefore, the local stream function can be evaluated by an integration of the above relations, e.g., $\psi = \int \rho u \mathrm{d}Y$ along a line of $X =$ constant. The maximum value of stream function ψ_m can be used to characterize the strength of the vortex rolls. Fig. 9 shows the predictions of the maximum value of stream function ψ_m varying with Ra at $As = 2.016$, and

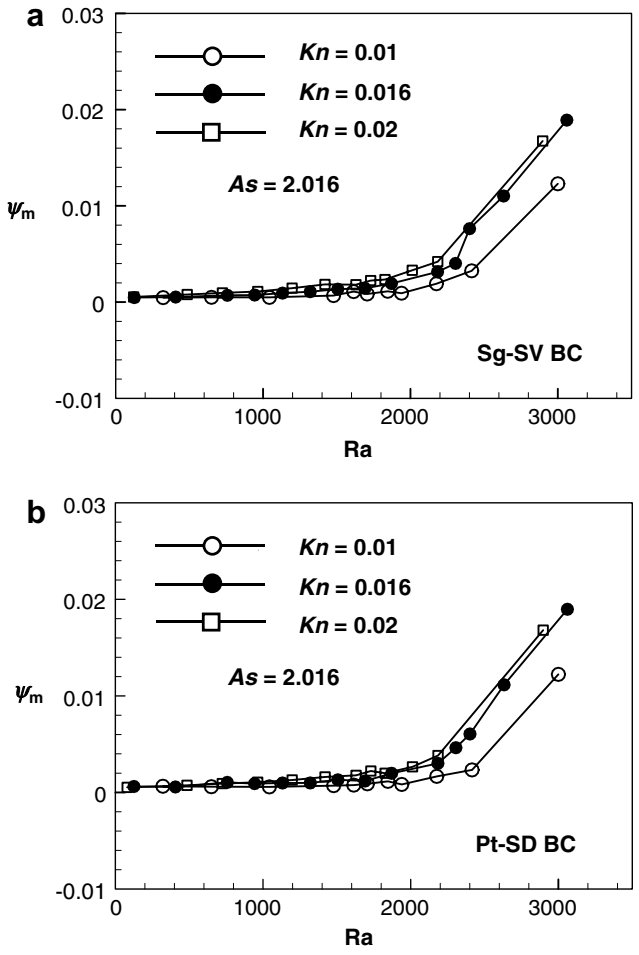

Fig. 9. Variation of maximum stream function ψ_m at various Ra and Kn in the enclosure of $As = 2.016$ with solid side wall conditions (a) Sg-SV BC and (b) Pt-SD BC.

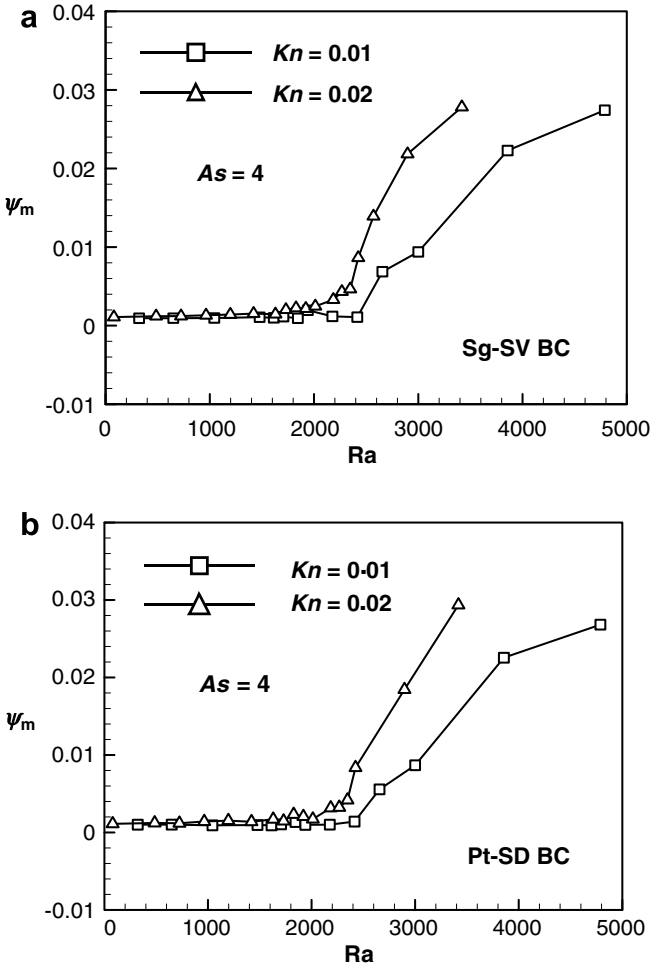

Fig. 10. Variation of maximum stream function ψ_m at various Ra and Kn in the enclosure of $As = 4$ with solid side wall conditions (a) Sg-SV BC and (b) Pt-SD BC.

$Kn = 0.01$, 0.016, and 0.02. Two solid wall conditions, Sg-SV BC and Pt-SD BC, generate very close results. It can be observed from the predictions presented in Fig. 9 that an increase in Kn causes premature convection state. However, in this case of smaller enclosure, the solid wall confinement effect is more salient and the onset of the instability appears mildly but not so abruptly like that for an infinitely extend fluid layer. To demonstrate this point, we present the predictions for the solid-wall enclosure of $As = 4$ in Fig. 10, where it is found that the influence of Kn has similar qualitative trend as the above case. As we addressed earlier, however, the onset of thermal instability from conduction to convection state occurs more dramatically under this configuration of weaker wall confinement. For the cases of $As = 4$ with the present side wall boundary condition, Pt-SD BC, the streamline pattern changes with the increasing Ra at Kn 0.01 and 0.02 are shown in Fig. 11. The detailed flow fields combining with the ψ_m data in Fig. 10, it can be observed that, for $As = 4$, the critical conditions are $Ra \approx 2400$ at $Kn = 0.01$ and $Ra \approx 2000$ at $Kn = 0.02$.

So far, with DSMC results presented above, we have disclosed that the two versions of adiabatic solid-wall conditions, Sg-SV and Pt-VD, generate solutions quite close to each other. However, the time-evolutions of thermal-fluid solutions are different in the two cases. In Fig. 12, we use a typical case of $Kn = 0.016$ and $Ra = 2632$ to address it. The DSMC simulation with Sg-SV BC settles down after 20,000th time step (N); while that with Pt-SD BC seems brought into steady state as earlier as about $N = 7000$. In Fig. 13, comparison of the solution histograms of various boundary conditions, the temperatures θ_R, θ_M, and $\bar{\theta}$ are monitored and presented. Fig. 13a shows a typical result with the SR BC. The computation converges to a steady state at the time step around $N = 12{,}000$. It is a simulation for periodic boundary condition rather than for adiabatic solid wall, but can be used in comparison with the computations with Sg-SV BC and Pt-SD BC conditions shown in Figs. 13b and c, respectively. It is found that the simulation with the Sg-SV BC evolves quite slow, while that with the present Pt-SD BC shows relatively faster evolution to the stationary state.

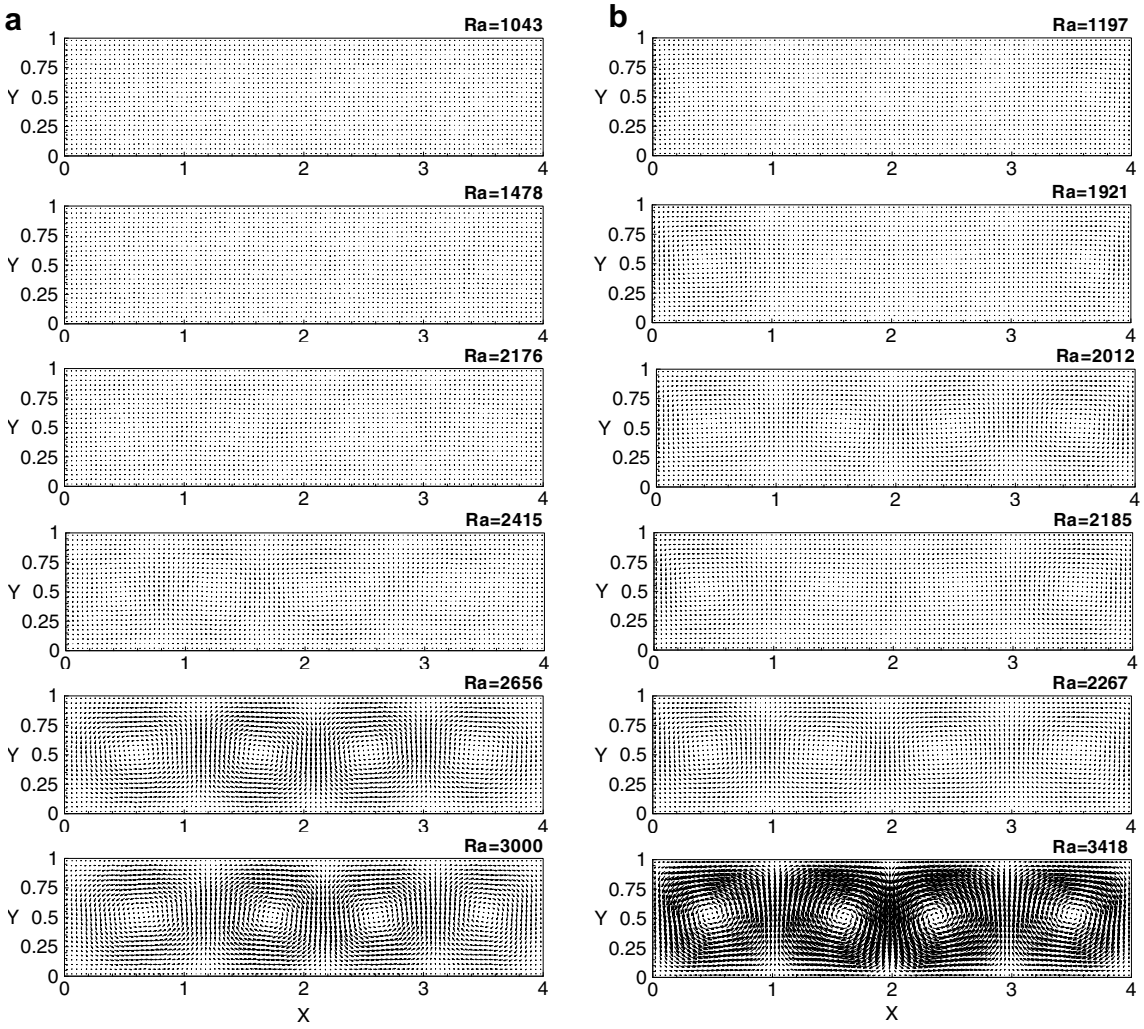

Fig. 11. Variation of steamline patterns of natural convection with Ra in the enclosure of $As = 4$ and sidewalls at Pt-SD BC. (a) $Kn = 0.01$; (b) $Kn = 0.02$.

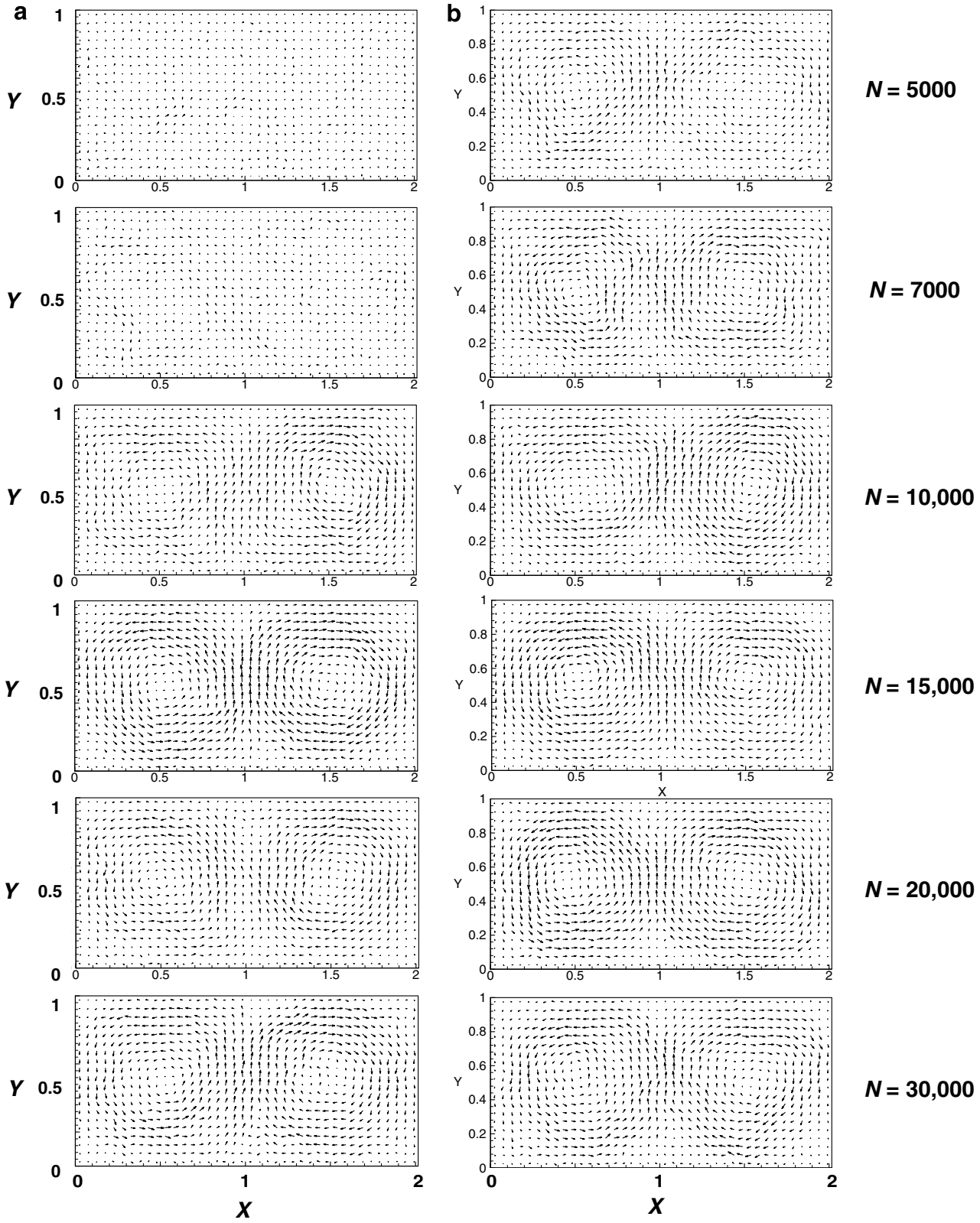

Fig. 12. Time-evolution of thermal-fluid field at $Kn = 0.016$ and $Ra = 2632$ in the enclosure of $As = 2.016$ with sidewalls at Sg-SV BC and Pt-SD BC.

Our result converges even faster than that with the simple SR BC for periodic boundaries. In addition, since there is no need to judge the segment type of the collision site like that in the Sg-SV BC, the Pt-SD BC proposed in the present paper is more physically realistic as well as renders the computation more efficient.

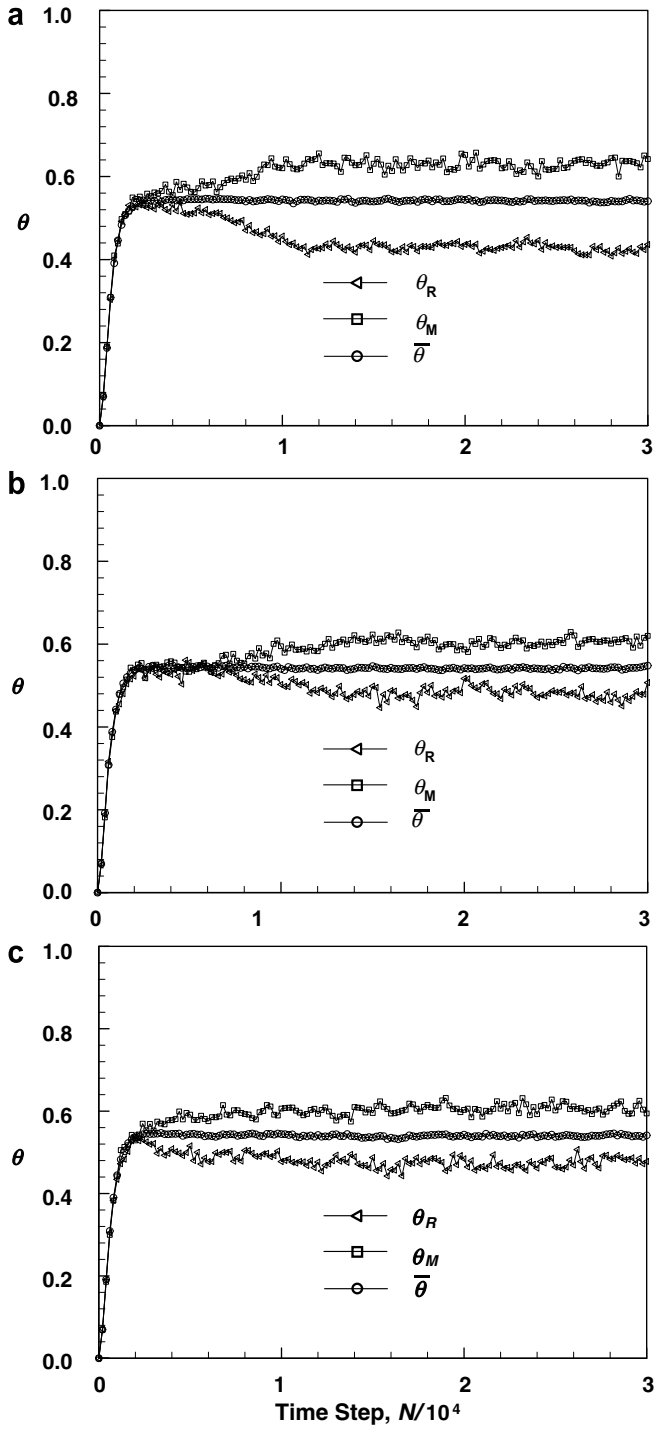

Fig. 13. Time-evolution of right wall temperature, middle point temperature, and the horizontal average temperature in the flow at $Kn = 0.016$ and $Ra = 2632$. (a) SR BC, (b) Sg-SV BC, (c) Pt-SD BC.

4. Concluding remarks

In the present work, a relatively novel wall-molecule collision rule for simulation of an adiabatic solid wall has been proposed and studied by using DSMC results of the Rayleigh–Bénard convection in a rectangular enclosure of adiabatic solid sidewalls. The present results demonstrated that the simulations with the previous hybrid condition (Sg-SV BC [26,27]) and the presently proposed Pt-SD BC generate reasonable predictions of critical condition and the thermal flow fields. In the parameter range considered in the present work, the simulations of the Rayleigh–Bénard thermal instability in solid enclosures of $As = 2.016$ and four have demonstrated that the increase in Kn may cause premature instability. The predictions with Sg-SV BC and Pt-SD BC agree very well in both qualitative and quantitative aspects. However, the novel treatment of wall-fluid molecular collision rule (Pt-SD BC) is more physically realistic and, based on the numerical experiment in the present work, it has been demonstrated that the novel Pt-SD BC leads computation to reach equilibrium more efficiently.

Acknowledgement

This research was partially supported by the National Science Council, the Republic of China under the Grant NSC 93-2212-E- 014-004.

References

[1] M. Gad-el-Hak, The MEMS Handbook, CRC Press, USA, 2002.
[2] G. Ciccotti, W.G. Hoover, Molecular-Dynamics Simulation of Statistical Mechanical Systems, North-Holland, Amsterdam, 1986.
[3] M.P. Allen, D.J. Tildesley, Computer Simulation of Liquids, Clarendon Press, Oxford, New York, 1990.
[4] J.M. Haile, Molecular Dynamics Simulation: Elementary Methods, Wiley, New York, 1992.
[5] G.A. Bird, Molecular Gas Dynamics and Direct Simulation of Gas Flow, Clarendon Press, Oxford, New York, 1994.
[6] E.S. Oran, C.K. Oh, B.Z. Cybyk, Direct simulation Monte Carlo: Recent advances and applications, Annu. Rev. Fluid Mech. 30 (1998) 403–441.
[7] G.A. Bird, The direct simulation Monte Carlo method: Current status and perspectives, in: M. Mareschal (Ed.), Microscopic Simulations of Complex Flows, Plenum Press, New York, 1990, pp. 1–13.
[8] G.E. Karniadakis, A. Beskok, Micro Flows: Fundamentals and Simulation, Springer-Verlag, New York, 2002, p. 257.
[9] S. Chandrasekhr, Hydrodynamic and Hydromagnetic Stability, Clarendon Press, Oxford, New York, 1961.
[10] K.T. Yang, Transitions and bifurcations in laminar buoyant flows in confined enclosures, ASME J. Heat Transf. 110 (1988) 1191–1203.
[11] E. Koschmieder, Bénard Cells and Taylor Vortices, Part I, Cambridge Univ. Press, Cambridge, England, UK, 1993.
[12] A.V. Gelting, Rayleigh–Bénard Convection: Structures and Dynamics, World Scientific, Singapore, 1998.
[13] E. Bodenschatz, W. Pesch, G. Ahlers, Recent developments in Rayleigh–Bénard convection, Annu. Rev. Fluid Mech. 32 (2000) 709–778.
[14] A.L. Garcia, Hydrodynamic fluctuations and the direct simulation Monte Carlo method, in: M. Mareschal (Ed.), Microscopic Simulations of Complex Flows, Plenum, New York, 1990, pp. 141–162.
[15] A.L. Garcia, C. Penland, Fluctuating hydrodynamics and principal oscillation pattern analysis, J. Stat. Phys. 64 (5/6) (1991) 1121–1132.
[16] S. Stefanov, C. Cercignani, Monte Carlo simulation of Bénard's Instability in a rarefied gas, Eur. J. Mech. B/Fluids 11 (5) (1992) 543–553.
[17] T. Watanabe, H. Kaburaki, M. Yokokawa, Simulation of a two-dimensional Rayleigh–Bénard system using the direct simulation Monte Carlo method, Phys. Rev. E 49 (5) (1994) 4060–4064.

[18] K. Yoshimura, T. Abe, Rarefaction effect on the Rayleigh–Bénard instability, AIAA 95-2055, Paper Presented at 30th AIAA Thermophysics Conference, June 19–22, San Diego, USA, 1995.
[19] E. Golshtein, T. Elperin, Convective instabilities in rarefied gases by direct simulation Monte Carlo method, J. Thermophys. Heat Transf. 10 (2) (1996) 250–256.
[20] T. Watanabe, H. Kaburaki, Particle simulation of three-dimensional convection patterns in a Rayleigh–Bénard system, Phys. Rev. E 56 (1) (1997) 1218–1221.
[21] H. Hirano, M. Seo, H. Ozoe, Two-dimensional numerical computation for Rayleigh–Bénard convection with both the Navier–Stokes equation and the Boltzmann equation, Model. Simul. Mater. Sci. Eng. 10 (2002) 765–780.
[22] S. Stefanov, V. Roussinov, C. Cercignani, Rayleigh–Bénard flow of a rarefied gas and its attractors. I. Convection regime, Phys. Fluids 14 (7) (2002) 2255–2269.
[23] S. Stefanov, V. Roussinov, C. Cercignani, Rayleigh–Bénard flow of a rarefied gas and its attractors. II. Chaotic and periodic convection regime, Phys. Fluids 14 (7) (2002) 2270–2288.
[24] P.Y. Tzeng, M.H. Liu, Direct simulation Monte Carlo modeling on two-dimensional Rayleigh–Bénard instabilities of rarefied gas, Num. Heat Transf. A 47 (8) (2005) 805–823.
[25] P.Y. Tzeng, M.H. Liu, Influence of number of simulated particles on DSMC modeling of micro-scale Rayleigh–Bénard flows, Int. J. Heat Mass Transf. 48 (14) (2005) 2841–2855.
[26] D.C. Rapaport, Time-dependent patterns in atomistically simulated convection, Phys. Rev. A 43 (12) (1991) 7046–7048.
[27] D.C. Rapaport, Unpredictable convection in A small box: molecular-dynamics experiments, Phys. Rev. A 46 (4) (1992) 1971–1984.
[28] K. Yamamoto, H. Takeuchi, T. Hyakutake, Characteristics of reflected gas molecules at a solid surface, Phys. Fluids 18 (2006) 046103.